Impact of the *R* and Mg on the structural, hydrogenation and magnetic properties of $R_{3-x}Mg_xCo_9$ (*R* = Pr, Nd, Tb and Y; $0 \leq x \leq 2$) compounds

Vitalii Shtender[1,2,3,*], Valérie Paul-Boncour[1], Roman Denys[4], Daniel Hedlund[5], Peter Svedlindh[5], Ihor Zavaliy[2]

[1]*Université Paris-Est, ICMPE (UMR7182), CNRS, UPEC, F-94320 Thiais, France*

[2]*Karpenko Physico-Mechanical Institute, NAS of Ukraine, 5 Naukova St., 79060 Lviv, Ukraine*

[3]*Department of Chemistry – Ångström Laboratory, Uppsala University, Box 538, 751 21, Uppsala, Sweden*

[4]*HYSTORSYS AS, P.O. Box 45, Kjeller NO-2027, Norway*

[5]*Department of Materials Science and Engineering, Uppsala University, Box 35, 751 03 Uppsala, Sweden*

*Corresponding Author

*E-mail: vitalii.shtender@kemi.uu.se

Abstract

R_2MgCo_9 (*R* = Pr, Nd, Tb and Y) compounds have been synthesized by a powder sintering method and **the** corresponding hydrides have been prepared by a solid gas method. Their crystal structure**s** and magnetic properties have been systematically studied. X-ray diffraction analysis showed that all R_2MgCo_9 compounds belong to the $PuNi_3$-type structure. The elements Tb, Y, Nd, Pr yield a lowering of the equilibrium pressure which correlates well with the increase **in** cell volume. The $R_2MgCo_9H(D)_x$ (*R* = Pr, Nd, Tb and Y; **($9.4 \leq x \leq 12$)**) hydrides (deuterides) preserve the $PuNi_3$-type structure with hydrogenation-induced volume expansion ranging from 14.7 to 19.6 %. **The substitution of** deuterium for hydrogen in R_2MgCo_9–$(H,D)_2$ (*R* = Tb and Y) prevents fast desorption at room temperature and ambient pressure. As for the magnetic properties, all **the** studied intermetallic compounds show ferromagnetic or ferrimagnetic behavior, **and** in some cases a temperature dependent spin reorientation. Hydrogen insertion reduces the magnetization and decreases the magnetic ordering temperature (T_C), whereas Mg for *R* substitution increases T_C.

Keywords: Rare **e**arth compounds, Magnesium compounds, Metal hydrides, Crystal structures, Magnetic properties.

1. Introduction

Modern society has great demand of functional materials for energy technologies **for** a sustainable future. Thus, detailed studies of new materials are highly prioritized. Among them, materials **with the ability to** store hydrogen by solid gas or electrochemical methods, offer new possibilities for energy storage.

Compounds with a $La_{2+n-x}Mg_xNi_{5n+4}$ **superlattice**, where *x* **(mainly $0 \leq x \leq 1$)** corresponds to the quantity of Mg substituting La in the Laves type layer and *n*=0-5 [1] have attracted interest as hydrogen absorbing materials and particularly as effective negative electrodes for Ni–*M*H secondary batteries [2–5]. The

electrochemical discharge capacity of La–Mg–Ni–Co alloys can reach 410 mAh/g, which is 30 % higher than the capacity of commercial $LaNi_5$-based electrodes [5]. Liao *et al*. studied the electrochemical performance of the $PuNi_3$ type $La_{3-x}Mg_xNi_9$ **($1 \le x \le 2.2$)** alloy series and found that the La_2MgNi_9 alloy exhibited the largest discharge capacity, the most rapid activation and a good high-rate discharge ability [6,7].

To date, only a few *R*–Mg–Co systems **have been** investigated mainly in terms of the formation of R_2MgCo_9/$R_{3-x}Mg_xCo_9$ **($0 \le x \le 2$)** and $RMgCo_4$/$R_{1-x}Mg_xCo_4$ **($0 \le x \le 1$)** compounds for hydrogen storage. The formation of extended $R_{3-x}Mg_xCo_9$ **($0 \le x \le 2$)** solid solutions was observed for *R*=Y [8], Nd [9], Tb [10] and Ce [11] alloys. These studies established that R_2MgCo_9 compounds adopt to the same structure type ($PuNi_3$-type and $R\bar{3}m$ space group) as the base binary RCo_3 compounds. The hydrogen storage capacity of the $Nd_{3-x}Mg_xCo_9$ **($0 \le x \le 1.5$)** alloys varies with Mg content and is in the range of 1.1-1.6 wt% H at room temperature and hydrogen pressures ≤ 10 bar [9]. However, the electrochemical discharge capacity of the $Nd_{3-x}Mg_xCo_9$-based electrodes does not exceed 100 mAh/g, which is less than 30 % of the hydrogenation capacity [9]. R_2MgCo_9 (*R*=Ce and Tb) compounds reversibly absorbs up to 1.4 wt. % H at room temperature and hydrogen pressures of 100 bar [12] and 25 bar [10], respectively. **Overall, the** hydrogen storage properties of R_2MgCo_9 compounds are comparable to that of the R_2MgNi_9 analogues.

In addition to significant hydrogenation capacity, $R_{3-x}Mg_xCo_9$ **($0 \le x \le 1.34$)** compounds show interesting magnetic properties. For example, partial substitution of a rare-earth element by Mg induces ferromagnetism in $Ce_{3-x}Mg_xCo_9$ **($0 \le x \le 1.34$)** [11,13] and increases the Curie temperature in Nd_2MgCo_9 **in comparison** to $NdCo_3$ [9]. Hydrogenation of Nd_2MgCo_9 causes a decrease **in** the transition temperature due to a weakening of the magnetic interactions and a change **in** ferromagnetic order towards antiferromagnetic order with T_N = 265 K and various spin reorientations at lower temperature [9].

Motivated by the fact that simple substitution of Ce for Mg in $Ce_{3-x}Mg_xCo_9$ **($0 \le x \le 1.34$)** [14] leads to a transition from a Pauli paramagnet to a strong ferromagnet, we have investigated other $R_{3-x}Mg_xCo_9$ **($1 \le x \le 2$)** systems. In this work, we present compounds with *R* = Pr, Nd, Tb and Y to show the influence of rare-earth element**s** and Mg on the hydrogenation properties, crystal structure of the parent compound and its hydrides as well as magnetic properties. The results obtained for these compounds are compared with those obtained earlier.

2. Experimental details

Starting materials for preparation of **the** R_2MgCo_9 (*R* = Pr, Nd, Tb, Y) alloys were ingots of *R* and Co (with purities ≥ 99.9%), and Mg powder (Alfa Aesar, 325 mesh, 99.8%). In the first step, binary R_2Co_9 and RCo_9 alloy precursors were prepared by arc melting in a purified argon atmosphere. The as-cast R_2Co_9 buttons were ground to **a** fine powder in an agate mortar and then mixed with Mg powder. Mg was added with 3 wt% excess in order to compensate for its evaporation loss at high temperatures. The powder mixtures were pressed into pellets, wrapped into tantalum foil, which were further loaded into a stainless-steel autoclave and sealed under **an** Ar atmosphere. Then, the samples were heated stepwise from 293 to 1073 K. Finally, the alloys were slowly cooled down to 773 K, annealed at this temperature for ~250 h and quenched in cold water. Phase structur**e**

analysis of the samples was carried out by powder X-ray diffraction (XRD) using a Bruker D8 diffractometer (Cu-Kα radiation).

The microstructure was evaluated with a Zeiss Merlin SEM equipped with a secondary electron (SE) detector and an energy-dispersive X-ray spectrometer (EDS). The samples for electron microscopy analysis were prepared by standard metallographic techniques through grinding with SiC paper. For the final polishing, a mixture of SiO_2 and water was used.

Hydrogen absorption/desorption properties of the alloys were characterized using a Sieverts type apparatus. The samples were activated by heating up to 473-523 K in dynamic vacuum, cooled to room temperature and then hydrogenated with high purity hydrogen gas (99.999%). Pressure–composition–temperature (*PCT*) curves were measured under H_2 pressures from 0.01 to 100 bar at different temperatures. The hydride sample holder was put into liquid nitrogen (77 K) for 30 minutes at a final internal pressure. Then the pressure in the sample-holder was gradually reduced to 1 bar and the hydrogenated samples **were** exposed to air, heated to room temperature and removed from the sample holder. Such **a** procedure was useful for samples with Tb and Y. It allows **passivation of** the surface by a thin oxide layer and avoid**s** fast hydrogen desorption at ambient pressure and temperature. Then the samples were transferred into small containers and placed in liquid N_2 or fridge to keep them for further investigations.

In situ Synchrotron Radiation XRD was carried out on the BM01B line at the European Synchrotron Radiation Facility (ESRF, Grenoble, France) using a monochromatic X-ray beam ($\lambda = 0.72085 \pm 0.00002$ Å). A thin quartz capillary (diameter 0.5 mm, wall thickness 0.01 mm) was filled by the investigated alloy powder (2–5 mg) and placed in a special quartz cell mounted on a goniometer head and connected to the gas system **by** a flexible plastic tube. The heating and cooling of the sample was performed using a programmable cryofluidic system with **a** working temperature range **of** 77–503 K. Initially the sample was heated in a dynamic vacuum to 423 K and at this temperature, the hydrogen gas (99.999% purity) was introduced into **the** quartz cell. Under these conditions, "activation" of the alloy was **carried out** and a solid solution of hydrogen in the intermetallic compound (IMC) was formed. Further, the sample was slowly cooled (5 K/min) to room temperature to achieve hydride formation.

Synchrotron radiation X-ray diffraction experiments have been performed at room temperature on the CRISTAL beam line of synchrotron SOLEIL for selected hydrides and deuterides. The powders were placed in glass capillaries (0.2-0.3 mm). The wavelength of the monochromatic beam, refined with a LaB_6 reference, was $\lambda = 0.6713$ Å. A Mythen multidetector has been used to obtain good statistics **over** a large Q range (1-12.7 $Å^{-1}$). Rietveld refinements of all XRD data were done with the FullProf suite software [15].

Magnetization measurements were carried out using a MPMS-5S SQUID magnetometer and a PPMS from Quantum Design. The samples were placed in gelatin capsules and fixed with glass wool. The diamagnetic contribution of the gelatin capsule (-2.8×10^{-8} emu/Oe) is negligible compared to the sample magnetization. Iso-magnetic field magnetization curves were recorded between 2 and 300 K with an applied field of 1 kOe. The measurements were in general performed with decreasing temperature. Isothermal magnetization curves were measured in the temperature range between 2 and 300 K with a maximum applied

field of 90 kOe. Additionally, magnetization versus temperature measurements for selected alloys were conducted using a LakeShore VSM in an applied field of 1 kOe from 300 to 800 K at a rate of 3 K/min.

3. Results and discussion

3.1. Crystal chemistry of the intermetallic compounds

IMCs with R_2MgCo_9 (*R* = Pr, Nd, Tb and Y) composition adopt the $PuNi_3$-type structure with $R\bar{3}m$ space group similar to the binary RCo_3. This structure type can be further described as stacking of Laves phase [A_2B_4] and $CaCu_5$-type Haucke phase [AB_5] layers along the [001] direction (A=*R*, Mg and B= Co). The results of crystallographic and energy-dispersive X-ray (EDX) investigations of the studied IMCs, their hydrides/deuterides as well as some literature data are presented in Table 1 and Figure 1. Herein and further we will mainly focus on the results for Pr_2MgCo_9 **compound** since it was studied in more detail. The Pr_2MgCo_9 composition is within $Pr_{3-x}Mg_xCo_9$ solid solution based on the binary $PrCo_3$ compound. The substitution of Mg for Pr occurs exclusively **at** the 6*c* crystallographic site in the Laves type layers [A_2B_4]. Pr atoms independently occupy the 3*a* position in the [AB_5] layers, while Co atoms are located **on** 3*b*, 6*c* and 18*h* sites. Thus, the studied R_2MgCo_9 (*R* = Pr, Nd, Tb and Y) IMCs are partially ordered compounds. Rietveld refinements of the synchrotron XRD data for Pr_2MgCo_9 and its hydride/deuteride are presented in Figure 1 and Table 2.

A different structure has been found for the $PrMg_2Co_9$ composition. The ternary $PrMg_2Co_9$ compound adopts the YIn_2Ni_9-type structure with tetragonal *P*4/*mbm* space group. Similar to Pr_2MgCo_9 **there is** one independent crystallographic position for Pr (2*a*) and three for **the** Co-atoms (8*j*, 2*c*, 8*k*). Ideally, the 4*g* position **is** filled with Mg-atoms only (as observed in $NdMg_2Co_9$ [9]), however, for the $PrMg_2Co_9$ compound we have found slight intermixing with Pr. Refined XRD data for $PrMg_2Co_9$ is presented in Figure SI1 (supporting information (SI)), the obtained crystallographic parameters are given in Table 2. A detailed comparison of the RMg_2Co_9 and R_2MgCo_9 structures can be found in [9].

As one may notice, RMg_2Co_9 compounds with YIn_2Ni_9-type structure have been found only for Nd [9] and Pr so far. Attempts to synthesize compounds of this composition with other *R* (*R*=Y, La, Ce, Tb) were not successful. **As for the $R_{3-x}Mg_xCo_9$ (*R* = Y, Ce, Pr, Nd and Tb) solid solutions, different concentration ranges were observed as a function of the rare earth. For the light rare earth elements, the solid solution spans up to $x \leq 1.5$ while for *R* = Y and Tb it is limited to $x \leq 1$.**

Table 1. Crystallographic parameters for the $R_{3-x}Mg_xCo_9$ (R = Pr, Tb, Y, Ce and Nd; $1 \leq x \leq 2$) alloys and their hydrides from Rietveld refinements of XRD data.

Alloy	Unit cell parameters			Hydride	Cell parameters			$\Delta a/a$ (%)	$\Delta c/c$ (%)	$\Delta V/V$ (%)	ΔV/at. H (Å^3)	Ref.
	a (Å)	c (Å)	V (Å^3)		a (Å)	c (Å)	V (Å^3)					
$R_{3-x}Mg_xCo_9$ (1≤ x ≤1.5) compounds and their hydrides ($PuNi_3$-type structure and $R\bar{3}m$ space group)												
Pr_2MgCo_9 **($Pr_{2.1(1)}Mg_{1.0(2)}Co_{8.9(2)}$)**	5.0415(1)	24.2405(5)	533.57(2)	$Pr_2MgCo_9H_{11.8}$ $Pr_2MgCo_9D_{\sim 12}$	5.3595(4) 5.36878(6)	25.420(2) 25.5608(4)	632.34(9) 638.05(1)	6.3 6.5	4.9 5.5	18.6 19.6	2.5 2.5	This work
$Pr_{1.5}Mg_{1.5}Co_9$	5.0047(2)	24.058(2)	521.84(6)	–	–	–	–	–	–	–	–	This work
Tb_2MgCo_9 **($Tb_{1.9(2)}Mg_{1.1(2)}Co_{9.0(1)}$)**	4.9855(3)	24.044(2)	517.55(7)	$Tb_2MgCo_9H_{\sim 10}$ $Tb_2MgCo_9D_{9.4}$	5.212(1) 5.2564(2)	25.232(7) 25.362(2)	593.5(3) 606.87(5)	4.5 5.4	4.9 5.5	14.7 17.3	2.5 3.2	This work
Y_2MgCo_9 **($Y_{2.1(1)}Mg_{1.1(1)}Co_{8.8(2)}$)**	4.9850(3)	24.087(2)	518.39(6)	$Y_2MgCo_9H_{11}$ $Y_2MgCo_9D_{10}$	5.262(1) 5.24072(6)	25.466(7) 25.3783(4)	610.5(3) 603.64(1)	5.6 5.1	5.7 5.4	17.8 16.5	2.8 2.8	This work
Ce_2MgCo_9 **($Ce_{2.0(1)}Mg_{1.1(1)}Co_{8.9(1)}$)**	4.9524(3)	24.258(3)	515.2(1)	$Ce_2MgCo_9D_{0.29}$	4.9615(3)	24.283(3)	517.69(9)	0.2	0.1	0.5	2.7	[12]
$Ce_{1.66}Mg_{1.34}Co_9$	4.923(1)	24.026(1)	504.3(1)	–	–	–	–	–	–	–	–	[11]
$Ce_{1.5}Mg_{1.5}Co_9$	4.9270(5)	23.969(3)	503.9(1)	–	–	–	–	–	–	–	–	This work
Nd_2MgCo_9 **($Nd_{2.1(1)}Mg_{1.0(1)}Co_{8.9(2)}$)**	5.0362(2)	24.1894(9)	531.32(3)	$Nd_2MgCo_9H_{11.4}$ $Nd_2MgCo_9D_{10}$	5.3267(2) 5.3272(4)	25.219(2) 25.368(4)	619.68(5) 623.5(1)	5.8 5.8	4.3 4.9	16.7 17.4	2.6 3.1	[9]
$Nd_{1.5}Mg_{1.5}Co_9$ **($Nd_{1.5(1)}Mg_{1.6(2)}Co_{8.9(2)}$)**	5.0017(4)	23.992(2)	519.78(7)	$Nd_{1.5}Mg_{1.5}Co_9H_{9.7}$	*Hydride immediately decomposed upon exposure to air*							[9]
RMg_2Co_9 compounds and their hydrides (YIn_2Ni_9-type structure and $P4/mbm$ space group)												
$PrMg_2Co_9$ **($Pr_{1.0(1)}Mg_{2.1(1)}Co_{8.9(1)}$)**	8.29452(7)	4.84304(5)	333.197(5)	–	–	–	–	–	–	–	–	This work
$NdMg_2Co_9$ **($Nd_{1.1(1)}Mg_{2.0(1)}Co_{8.9(2)}$)**	8.2789(2)	4.8368(2)	331.51(2)	$NdMg_2Co_9H_{3.5}$	*Hydride immediately decomposed upon exposure to air*							[9]

Compositions in parentheses are from EDX experiments.

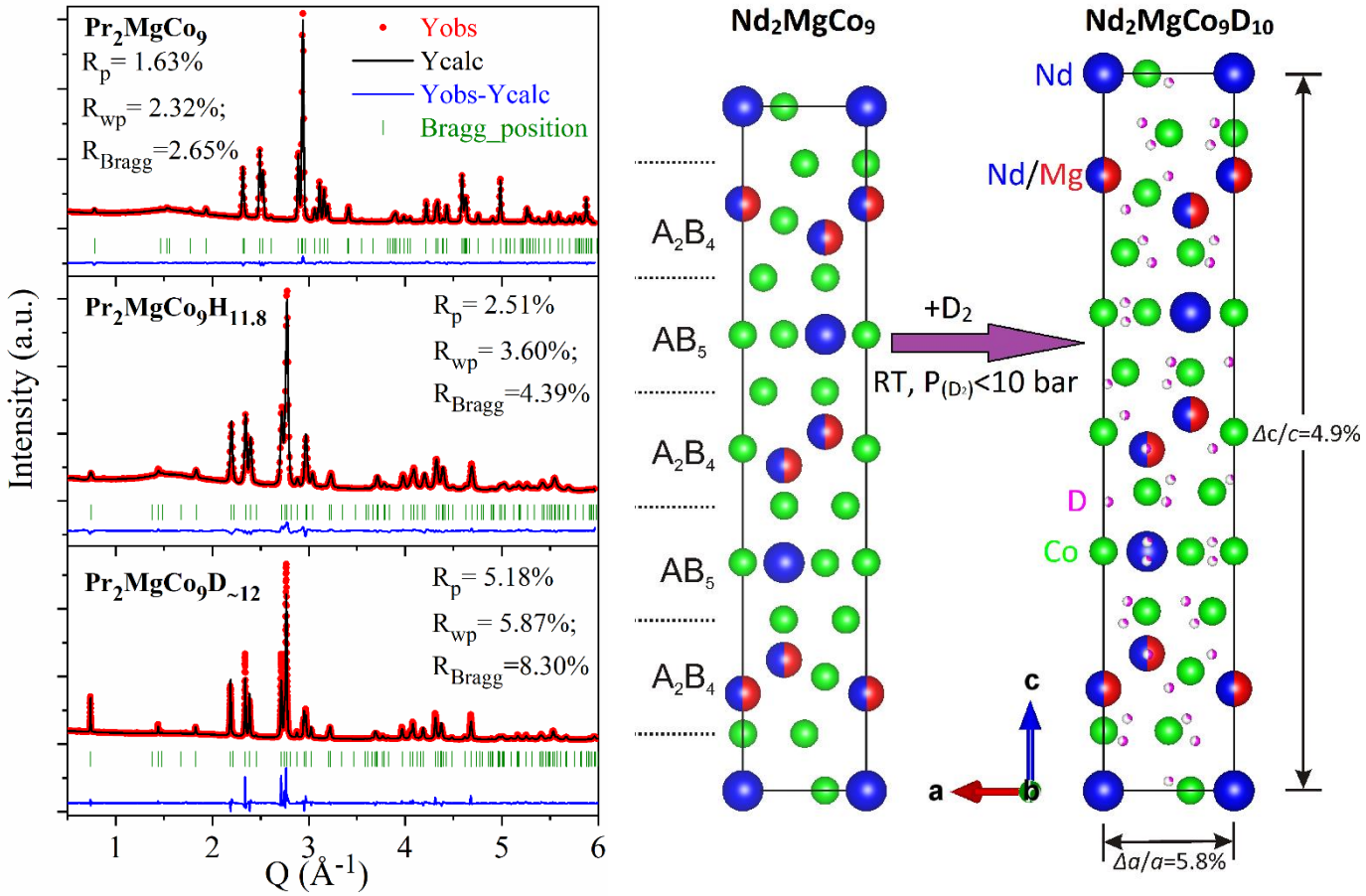

Figure 1. *(left)* Synchrotron powder X-ray diffraction patterns of Pr_2MgCo_9 and its hydride/deuteride. *(right)* Projections of the Nd_2MgCo_9 and its deuteride unit cell on the *ac* plane.

3.2. Hydrogen absorption/desorption properties

The Pr_2MgCo_9 compound readily absorbed up to 12.9 hydrogen atoms per formula unit (H at./f.u.) or 1.53 wt.% at 293 K and 10 bar pressure (Figure SI2(*left*)). When the hydrogen pressure was lowered down to 1 bar, partial hydrogen desorption down to 1.4 wt.% H (11.8 H at./f.u.) was observed.

Measurements of pressure-composition-isotherms (*PCI*) showed complete reversibility of hydride formation by R_2MgCo_9. Figure 2(*left)* shows room temperature *PCI* for the Pr_2MgCo_9-D_2 system. A flat and wide pressure plateau is observed around 0.1 bar D_2 with relatively small absorption-desorption hysteresis.

The equilibrium pressures of hydrogen absorption-desorption for R_2MgCo_9 (*R* = Tb, Y) are **an** order of magnitude higher than for Pr_2MgCo_9 (Figure SI2 (*right*) and Figure 2 (*right*)). Such behavior correlates well with cell volume differences (the plateau pressure increases as the cell volume decreases). Here, the different unit cell dimensions are related to different *R* radii, whereas for $Nd_{3-x}Mg_xCo_9$ **($1 \leq x \leq 1.5$)** solid solution [9], the cell volume variations are related to different Mg concentrations. The R_2MgCo_9 (*R* = Tb, Y) compounds absorb around 10 H at./f.u. at room temperature and 12 bar hydrogen pressure. Higher hydrogen concentration**s** can be reached in these compounds by applying higher pressure but when the pressure is released, they very easily desorb hydrogen. Isotherms of hydrogen desorption by $Y_2MgCo_9H_x$ have been measured at three different temperatures in order to determine its thermodynamic stability (Fig. 2 (*right*)). The following thermodynamic parameters have been obtained from the van't Hoff dependencies: the enthalpy

change ΔH_{des}=33.8±0.3 kJ/mol and the entropy change ΔS_{des}=119.1±0.9 J/(mol K). These values are comparable to parameters obtained for Nd_2MgCo_9–H_2 (ΔH_{des}=39.1±0.2 kJ/mol and ΔS_{des}=120±0.5 J/(mol K)) [9] and Ce_2MgCo_9–H_2 (ΔH_{des}=27.2±0.2 kJ/mol and ΔS_{des}=120.9±0.8 J/(mol K)) [12]. From the values of ΔH_{des} one can notice that the stability of the hydrides increases from **Ce to Y then to Nd**.

Table 2. Crystal structure data for the Pr_2MgCo_9, $Pr_2MgCo_9H_{11.8}$, $Pr_2MgCo_9D_{12}$ and $PrMg_2Co_9$ compounds **obtained** from Rietveld refinements of XRD and synchrotron XRD data.

Refined composition: **$Pr_{2.10(1)}Mg_{0.90(1)}Co_9$**					
$PuNi_3$-type, sp. gr. $R\bar{3}m$; a = 5.04152(9) Å; c = 24.2405(5) Å; V = 533.57(2) Å^3; Z = 3					
R_{Bragg} = 2.65 %					
Atom	Site	x	y	z	B_{iso} (Å^2)
Pr1	3*a*	0	0	0	0.70(3)
0.45(3)Mg/0.55(3)Pr2	6*c*	0	0	0.14210(5)	1.05(5)
Co1	3*b*	0	0	1/2	0.72(2)
Co2	6*c*	0	0	0.33371(8)	0.72(2)
Co3	18*h*	0.5011(2)	–*x*	0.08315(5)	0.72(2)
$Pr_{2.10}Mg_{0.90}Co_9H_{11.8}$					
$PuNi_3$-type, sp. gr. $R\bar{3}m$; a = 5.3595(4) Å; c = 25.420(2) Å; V = 632.34(9) Å^3; Z = 3					
R_{Bragg} = 4.39 %					
Atom	Site	x	y	z	B_{iso} (Å^2)
Pr1	3*a*	0	0	0	1.73(8)
0.45(-)Mg/0.55(-)Pr2	6*c*	0	0	0.1421(1)	3.1(1)
Co1	3*b*	0	0	1/2	2.38(6)
Co2	6*c*	0	0	0.3326(2)	2.38(6)
Co3	18*h*	0.4933(4)	–*x*	0.0808(1)	2.38(6)
$Pr_{2.10}Mg_{0.90}Co_9D_{\sim 12}$					
$PuNi_3$-type, sp. gr. $R\bar{3}m$; a = 5.36878(6) Å; c = 25.5608(4) Å; V = 638.05(1) Å^3; Z = 3					
R_{Bragg} = 8.30 %					
Atom	Site	x	y	z	B_{iso} (Å^2)
Pr1	3*a*	0	0	0	1.57(4)
0.45(-)Mg/0.55(-)Pr2	6*c*	0	0	0.14101(7)	2.39(4)
Co1	3*b*	0	0	1/2	1.53(3)
Co2	6*c*	0	0	0.3322(1)	1.53(3)
Co3	18*h*	0.4919(2)	–*x*	0.07883(5)	1.53(3)
Refined composition: **$Pr_{1.05(1)}Mg_{1.95(1)}Co_9$**					
YIn_2Ni_9-type; sp. gr. $P4/mbm$; a = 8.29452(7) Å; c = 4.84304(5) Å; V = 333.197(5) Å^3; Z = 2					
R_{Bragg} = 7.54 %					
Atom	Site	x	y	z	B_{iso} (Å^2)
Pr1	2*a*	0	0	0	0.50(3)
0.975(3)Mg/0.025(3)Pr2	4*g*	0.6190(4)	*x*+1/2	0	1.0(1)
Co1	8*j*	0.0662(2)	0.2145(2)	1/2	0.20(2)
Co2	2*c*	0	1/2	1/2	0.20(2)
Co3	8*k*	0.1790(2)	*x*+1/2	0.2465(3)	0.20(2)

Statistical mixtures of Mg/Pr were taken as it was calculated for the IMC and fixed for the hydride and deuteride.

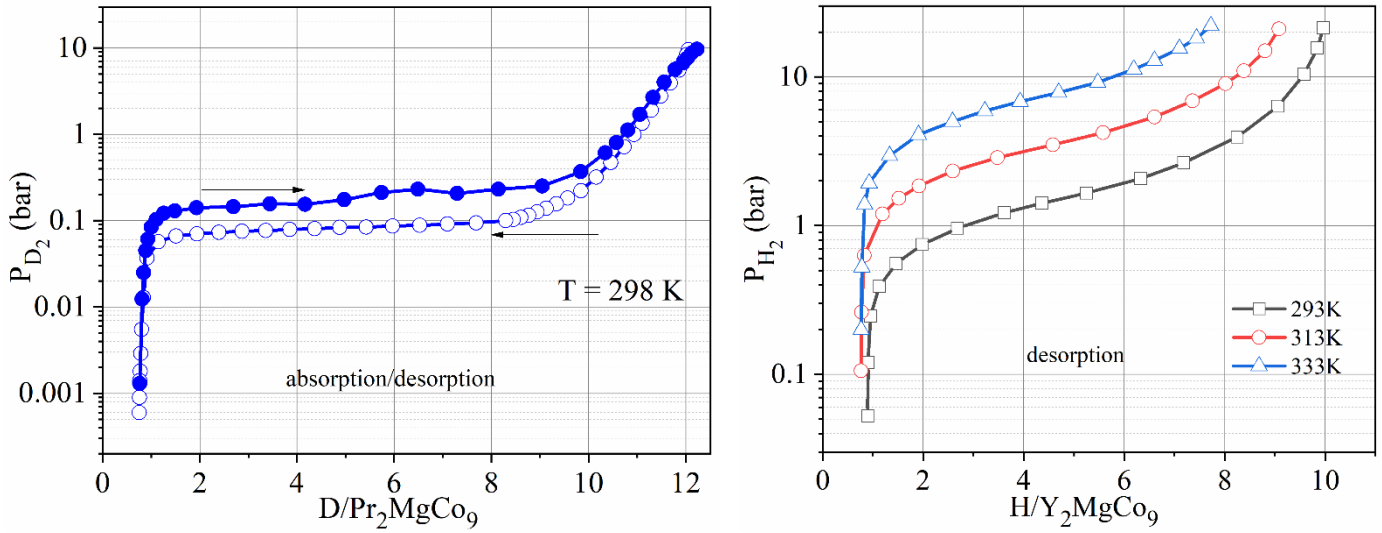

Figure 2. (*left*) Absorption/desorption *PCI* for Pr_2MgCo_9–D_2 and (*right*) desorption *PCT* for Y_2MgCo_9–H_2.

3.3. Structural characteristics of the hydrides/deuterides

Earlier in [9,10,12] it was shown that R_2MgCo_9 hydrides/deuterides retain the trigonal structure of the parent compounds with a volume expansion of 14.7–19.6 %. Interestingly, atom positions remain almost unchanged after hydrogen/deuterium uptake, **and** only cell expansion in the range 4.3-6.5 % was observed. All crystallographic details for hydrides/deuterides are gathered in Tables 1 and 2 with **a** graphical **representation** in Figure 1. Nd_2MgCo_9 and its deuteride have been chosen for graphical visualization as the structure of $Nd_2MgCo_9D_{10}$ was studied earlier [9] and the exact location of D-atoms was established (see Figure 1(*right*)). D atoms partially occupy four types of interstices, including octahedral Nd_2Co_4 sites, tetrahedral Nd_2Co_2 sites and two types of trigonal bipyramids $(Nd,Mg)_3Co_2$. A more detailed description of the crystal structure of $Nd_2MgCo_9D_{10}$ and **a** comparison with similar members can be found in [9].

Increasing the Mg-content decreases the thermodynamic stability of the hydrides and thus the crystal structures of $R_{1.5}Mg_{1.5}Co_9H_y$ and $RMg_2Co_9H_y$ remain unknown [9]. However, it can be can assumed that these hydrides should follow established trends for $R_{3-x}Mg_xCo_9H_y$ **($0 \leq x \leq 1.5$)** [9] and $RIn_2Ni_9H_y$ [16], where hydrides keep the parent structure of the IMC with some volume expansion. **Due to the low quality of $Ce_{1.5}Mg_{1.5}Co_9$, which was multiphase, we have not synthetized the corresponding hydride. $Ce_{1.66}Mg_{1.34}Co_9$ was studied in [11] only for magnetic properties but not for hydrogen storage properties. It was also assumed that both $Pr_{1.5}Mg_{1.5}Co_9H_y$ and $PrMg_2Co_9H_y$ have low stability similarly to Nd-containing compounds.**

Hydrides of R_2MgCo_9 compounds with R = Tb and Y have been found **to be** significantly less stable compared to hydrides based on Pr- and Nd-containing compounds. It correlates with **a** smaller unit cell due to **the** lanthanide contraction and thus increasing equilibrium pressure which is above atmospheric pressure for compounds with Tb and Y. A short *in-situ* hydrogenation process has been performed to demonstrate structural changes in the Y_2MgCo_9–H_2 system. A single step transformation from IMC to hydride was observed (Figure SI3) without changing the structural parameters (only cell expansion). We therefore found that deuterides of R_2MgCo_9 (R = Tb and Y) are more resistant to desorption than corresponding hydrides and studying their crystal structures is much easier with inhouse conditions. This isotope effect is caused by lower equilibrium

pressure for systems with deuterium. Earlier, similar behavior **was observed** for the $TbMgNiCo_3$–$(H,D)_2$ system [17] where the corresponding γ-deuteride **kept** its structure at atmospheric pressure whereas with hydrogen only the β-hydride was not decomposed.

3.4. Magnetic properties of the $R_{3-x}Mg_xCo_9$ IMC and their hydrides/deuterides

To start off, we would like to **provide** additional information **regarding** some of the features **in** the magnetic results of $R_{3-x}Mg_xCo_9$ **($1 \leq x \leq 2$)** at higher temperatures, to avoid further misunderstandings in interpreting the result**s**. As will be seen below, the magnetization of these compounds does not approach zero after heating above the Curie temperature (T_C). Firstly, the difficulty is that some oxidation can occur upon heating, thus inducing a **partial** decomposition into ***R*-*oxide***, Mg-oxide and Co. Secondly, some of the parent compounds (RMg_2Co_9 (R=Pr and Nd), $Nd_{1.5}Mg_{1.5}Co_9$ and Y_2MgCo_9) contain **few** magnetic impurities (R_2Co_{17} (R= Pr and Nd), $NdCo_5$ and $YMgCo_4$) which have **a** T_C of 1168 K for Pr_2Co_{17} [18], 1181 K for Nd_2Co_{17} [19], 913 K for $NdCo_5$ [20] and 404 K for $YMgCo_4$ [unpublished results].

Fig. 3 presents a comparison of the magnetization versus temperature and applied magnetic field curves for the R_2MgCo_9 (R= Y, Pr, Nd and Tb) compounds. Y_2MgCo_9 displays a ferromagnetic behavior with a T_C of 643 K, where the feature at ~400 K can be related to the ferromagnetic transition of $YMgCo_4$ at 404 K [unpublished results]. The saturation is still not reached at 90 kOe and 2 K, indicating a significant magnetocrystalline anisotropy and a possible metamagnetic transition at even larger magnetic fields. The magnetization extrapolated at low field yields 8.2 μ_B/f.u., which gives, assuming a collinear ferromagnetic structure, an average Co moment of 0.9 μ_B/atom. For comparison, in YCo_3 successive metamagnetic transitions **were** observed with a Co moment at 10 K changing from 0.60 μ_B/Co below 0.2 MOe to 1.23 μ_B at 0.9 **MOe** [21]. A neutron analysis revealed that YCo_3 has a ferrimagnetic ground state (Co2 moment is antiparallel to Co1 and Co3) and undergoes metamagnetic transitions towards a ferromagnetic state with a mean Co moment of 1.16 μ_B/Co at high field [22]. In addition, YCo_2 has a very weak moment at low field and undergoes a metamagnetic transition towards a metamagnetic state around 0.7 MOe with 0.44 μ_B/Co at 10 K and above 0.7 **MOe** [23], whereas in $YMgCo_4$, the mean Co moment is 1.26 μ_B/Co atom at 4.2 K [unpublished results]. This indicates that substituting Mg for Y enhances the Co moment at a moderate field.

The inset in Fig. 3(*right*) shows a comparison of the hysteresis loops for the three alloys at 2 K. The compounds with R = Nd and Tb have a coercive field H_C between 300 and 400 Oe, whereas it reaches H_C = 1400 Oe for Y.

Pr_2MgCo_9 displays reduction **of the magnetization** at 109 K but remains ferromagnetic with T_C above room temperature (Fig. 4). Assuming a collinear spin structure for the alloy with a Pr moment of 3.5 μ_B/Pr atom and Co moments of 0.9 μ_B/Co, a total magnetization of 15.1 μ_B is obtained, not far from the experimental value at 10 K (15 μ_B/f.u.). Deuterium absorption induces a decrease of the magnetization and T_C. The comparison of the $M(H)$ curves shows a decrease of the saturation magnetization from 15 to 5 μ_B/f.u. upon deuteriation whereas the coercivity increases in the deuterated sample. At 300 K, the alloy is still in the ferromagnetic region as T_C is 649 K (Fig 3 (*left*)). The decrease of the magnetization for the deuterated sample

can originate from a canted magnetic structure between the Pr and Co moments. A reduction of the ordering temperature is often observed in hydrides due to a decrease of the *R*-Co interactions upon an increase of the interatomic distances by hydrogen insertion [24].

Concerning Nd_2MgCo_9 [9], a maximum is found at 250 K, which is tentatively assigned to a spin reorientation whereas its T_C is 638 K (similar behavior was observed also for $NdCo_3$ [25]). The analysis of the magnetization curve at 2 K shows an extrapolated magnetization of 14.2 μ_B/f.u. at 5 T. A simple calculation assuming a Nd moment of 3.5 μ_B and a ferromagnetic structure with $\mu_{Co} = 0.9\mu_B$ yields 15.1 μ_B/f.u., which is not far from the experimental value. The finite slope of the magnetization above 5 T indicates a further alignment of the magnetic moments.

Tb_2MgCo_9 shows a minimum **of the magnetization** around 300 K followed by an increase **towards** a maximum at 574 K and a Curie temperature of 709 K. A plausible explanation is that Tb_2MgCo_9 orders ferrimagnetically and exhibits a compensation temperature around 300 K. At 2 K, the extrapolated magnetization is only 4 μ_B/f.u., which assuming a Tb moment of 9.5 μ_B/atom with antiparallel and colinear alignment of Tb and Co moments, leads to a mean value for the Co moment of 1.67 μ_B/Co. This value is too large compared to other isostructural compounds (0.9 μ_B/Co) and indicates canted Tb moments and/or a reduction of the Tb moment by crystal field effects.

One can notice that **the** crystal structure of these compounds is composed **by the stacking** of $[AB_5]$ and $[A_2B_4]$ layers, with three independent positions for cobalt, one for rare-earth element **only and one** mixed Mg/*R* position. Such packing could affect the behavior of magnetic atoms during the heating together with different expansions of the sublattices. As can be seen in Table 3, except for Tb_2MgCo_9, the experimental magnetization results for the R_2MgCo_9 (*R*= Y, Pr and Nd) compounds show good agreement with calculated values for the magnetization described in a ferromagnetic structure. The expected magnetization was calculated assuming a ferromagnetic collinear structure and literature values for the atomic magnetic moments. Additional experiments such as neutron diffraction measurements are required to correctly describe the magnetic structure of Tb_2MgCo_9.

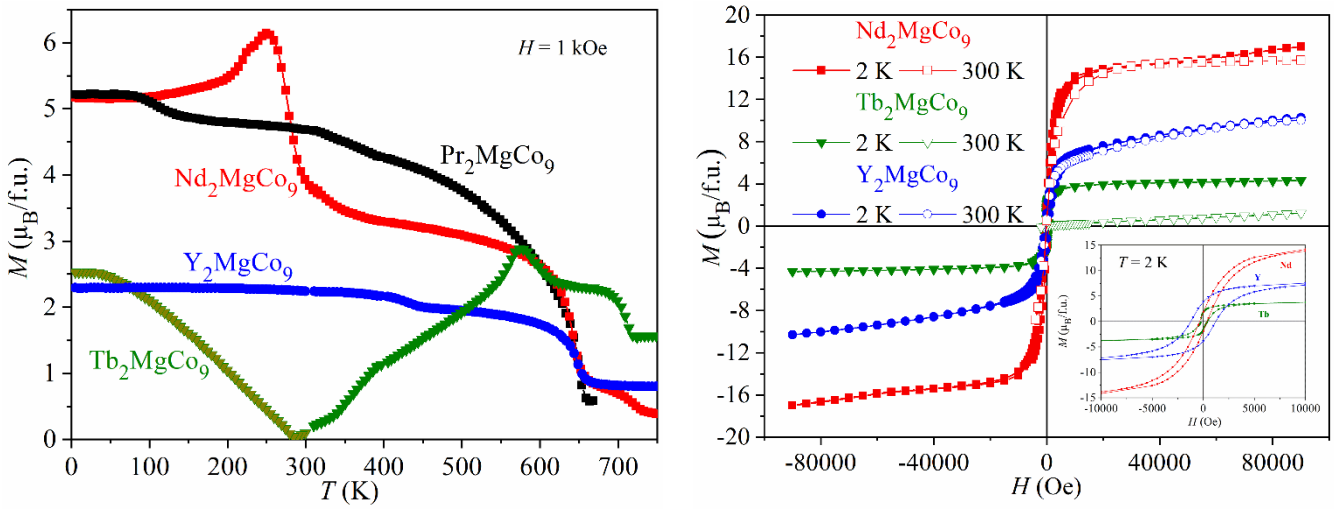

Figure 3. (*left*) *M*(*T*) at 1 kOe and (*right*) *M*(*H*) curves at 2 K and 300 K for the R_2MgCo_9 (*R* = Y, Pr, Nd, Tb) compounds. The inset shows a comparison of *M*(*H*) curves at 2 K.

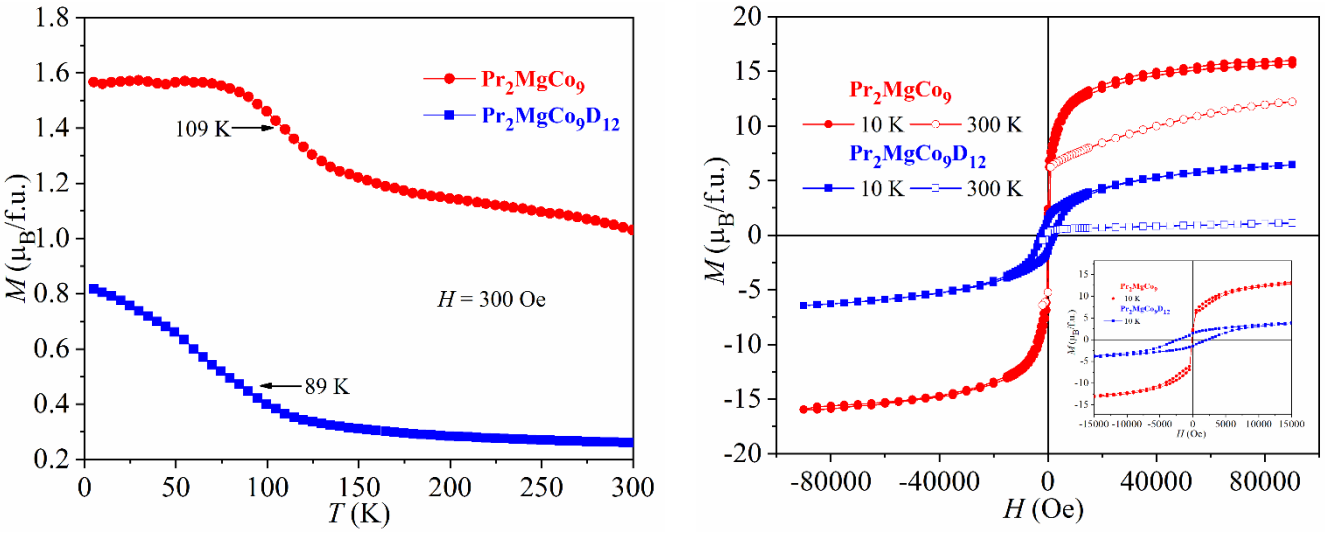

Figure 4. (*left*) *M*(*T*) at 300 Oe and (*right*) *M*(*H*) curves at 10 K and 300 K for the Pr_2MgCo_9 compound and its deuteride. The inset represents a zoom for the curves at 10 K.

Table 3. Summary **of** the magnetization of the R_2MgCo_9 (*R*= Y, Pr, Nd and Tb) compounds at 2K. The expected magnetization was calculated assuming a ferromagnetic collinear structure and literature values of the atomic magnetic moments (0.9 μ_B/Co, 3.5 μ_B/*R* (*R*=Pr and Nd) and 9.5 μ_B/Tb [26]).

Compound	Expected magnetization (μ_B/f.u.)	Measured magnetization (μ_B/f.u.)
Y_2MgCo_9	8.1	8.2(1)
Pr_2MgCo_9	15.1	15.0(1)
Nd_2MgCo_9	15.1	14.2(1)
Tb_2MgCo_9	10.9	4.0(1)

A selection of alloys from a previous study, $Nd_{3-x}Mg_xCo_9$ **($0.45 \leq x \leq 2$)** and $NdMg_2Co_9$, were additionally investigated by magnetometry to show the effect of *R* and Mg on the magnetic properties for a larger series of compounds (Fig. 5). The main purpose was to investigate the change in T_C, however this is further complicated by a magnetic R_2Co_{17} impurity phase. Fig 5(*left*) demonstrates an increasing T_C from Y → Pr → Nd→ Tb for binary RCo_3 and also for R_2MgCo_9. Notably, T_C*s* of Mg-based compounds are higher by 200-300 K compared to the binaries. In Fig. 5 (*right*), the $T_C(x)$ curves of the $Nd_{3-x}Mg_xCo_9$ **($0 \leq x \leq 2$)** and $Ce_{3-x}Mg_xCo_9$ **($0.43 \leq x \leq 1.34$** [11,13]) compounds are presented, showing an increase of $\boldsymbol{T_C}$ with increasing Mg-content. It should be noted that for $x = 2$, we have observed a different crystal structure, which is likely the main reason for the lower T_C **value which does** not follow the trend of increasing Curie temperature. Similar behavior is observed for $Pr_{3-x}Mg_xCo_9$ ($x = 1$ and 2) compounds shown in Fig. SI4 (*right*). Additionally, hydrogen reduces the magnetization and decreases $\boldsymbol{T_C}$for both types of compounds (with Mg and without). The only exception is $CeCo_3H_4$ where a T_C of 80 K was measured while $CeCo_3$ is a Pauli paramagnet [11]. All of these results are also listed in Table SI1.

As a final remark on the magnetic results, we would like to draw attention to the influence of Mg on the magnetic properties of $R_{3-x}Mg_xCo_9$ **($0 \leq x \leq 2$)** compounds and how it could help to understand our results.

The effect of *R* and H insertion is not unexpected and covered earlier in this section, so we will focus on the influence of Mg alloying. Firstly, experimentally [11] it was shown that Mg substitution in $Ce_{3-x}Mg_xCo_9$ **($0 \leq x \leq 1.34$)** transforms $CeCo_3$ from a Pauli paramagnet to a ferromagnet with a large monocrystalline anisotropy and a T_C above 400 K. In other words, it was transformed into a compound which has some of the necessary requisites for a permanent magnet. This transformation is at first sight unexpected, but Pandey and Parker [14] described from a theoretical perspective how these changes come about. They highlighted that the origin of this magnesium induced ferromagnetism could be described using the Stoner criterium for itinerant ferromagnetism and that alloying with Mg increases the Fermi-level density of states $N(E_F)$. It was also shown that $CeCo_3$ was near a ferromagnetic instability, $IN(E_F) \sim 0.98$, where *I* denotes the Stoner exchange parameter, whereas the Stoner criterion for ferromagnetism is $IN(E_F)>1$; alloying with Mg then pushes $IN(E_F)$ above 1, **stabilizing** a ferromagnetic ground state.

As mentioned in both the experimental [11,13] and theoretical [14] descriptions, it highlights that alloying with Mg could push materials **which are near** a ferromagnetic instability **towards** stable **ferromagnetic state**, i.e. to rehabilitate failed magnetic materials to be viable as permanent magnets. Quoting Canfield [27], "We think that this idea of rehabilitation is worthy of much greater attention, opening up a whole new strategy for finding new magnetic materials", we have here another possible example of this. We have shown that Mg-**substitution in** various RCo_3 binary compounds increases T_C to a large extent. However, these compounds are already in a magnetically ordered state, but the significant increase in T_C is satisfying. One should also note that Mg substitution reduces the cell volume of the $R_{3-x}Mg_xCo_9$ **($0 \leq x \leq 1.5$)** compounds, which can cause stronger *R*-Co and Co-Co interactions which will **further** affect the magnetic behavior. To support this for our compounds, similar work as presented in the theoretical description [14] of Mg-alloyed $CeCo_3$ would be beneficial, but is outside the scope of this work.

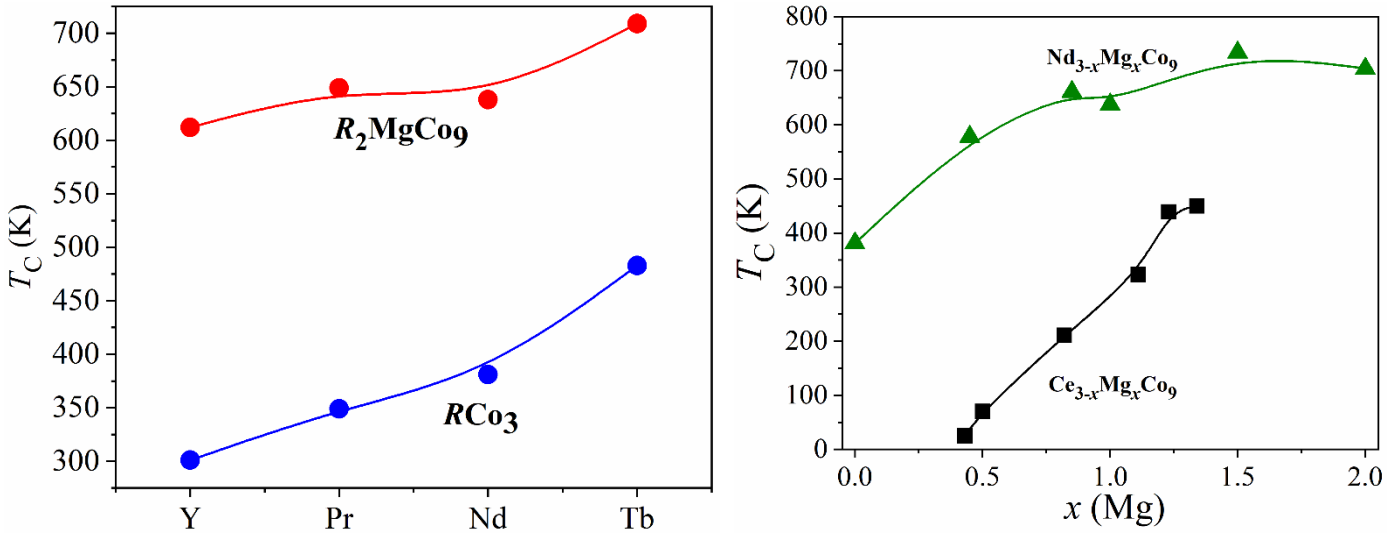

Figure 5. (*left*) T_C *vs.* *R* for RCo_3 and R_2MgCo_9 (*R*= Y, Pr, Nd and Tb) compounds and (*right*) T_C *vs.* Mg for $R_{3-x}Mg_xCo_9$ (*R*= Ce and Nd**; ($0 \leq x \leq 2$)**) compounds.

4. Conclusions

In this work we have investigated the structural, hydrogenation and magnetic properties of R_2MgCo_9 (R = Pr, Nd, Tb and Y) ternary compounds and their hydrides/deuterides. R_2MgCo_9 intermetallics exhibit a $PuNi_3$-type structure with $R\bar{3}m$ space group **as observed in** the binary RCo_3 compounds. Intermetallics with the RMg_2Co_9 composition have **only** been identified so far for Nd and Pr with the unique structure (YIn_2Ni_9-type; sp. gr. $P4/mbm$). The unit cell volume of the $R_2MgCo_9/R_{3-x}Mg_xCo_9$ **($0 \leq x \leq 1.5$)** compounds decreases with decreasing atomic radius of R and increasing Mg content. This phenomenon is significant for hydrogenation since the corresponding plateau pressure at a given temperature increases and the thermodynamic stability of the hydrides decreases. Hydrides/deuterides retain the structure of the parent compound with a significant cell volume increase. The deuterium for hydrogen substitution in the $R_2MgCo_9-(H,D)_2$ (R = Tb and Y) systems prevents fast desorption at room temperature and ambient pressure. As for the magnetic properties **of** the studied compounds, some intermetallic compounds are ferromagnetic (R = Y, Nd, Pr) or ferrimagnetic (R = Tb) with high Curie temperatures. However, a spin reorientation is observed for Nd_2MgCo_9 and a compensation point around room temperature with maximum at 574 K for Tb_2MgCo_9. The Curie temperature T_C for the studied $R_2MgCo_9/R_{3-x}Mg_xCo_9$ **($0.45 \leq x \leq 2$)** compounds can be tuned by controlling the Mg content and by changing **the** R element while insertion of H or D decreases the saturation magnetization and transition temperatures in the presented $R_2MgCo_9/R_{3-x}Mg_xCo_9$ **($0 \leq x \leq 1$)** compounds.

In the presented study we once more showed an interesting effect of Mg on the magnetic properties in $R_{3-x}Mg_xCo_9$ **($0 \leq x \leq 2$)** systems. Mg acts as a lever for pushing up T_C in R_2MgCo_9 (R = Pr, Nd, Tb, Y) and $Nd_{3-x}Mg_xCo_9$ **($0 \leq x \leq 2$)** compounds. Theoretical calculations together with neutron diffraction studies are of interest for achieving a detailed description of the magnetic properties for the compounds presented in this work.

Conflicts of interest

There are no conflicts to declare.

Acknowledgments

This research was done thanks to the synchrotron beam times allocated by the synchrotron at ESRF and SOLEIL. This work was supported partially by the French government scholarship program for short-term research visits in 2014 (No. 815302G). Part of the results **were** obtained by V. Shtender within the postdoctoral stay at ICMPE, Project ID: PRESTIGE-2017-2-0002. The authors are thankful to Rebecca Clulow for proofreading of the manuscript.

References

[1] H. Hayakawa, E. Akiba, M. Gotoh, T. Kohno, Crystal structures of La–Mg–Ni_x (x = 3-4) system hydrogen storage alloys, Mater. Trans. 46 (2005) 1393–1401. doi:10.2320/matertrans.46.1393.

[2] Y. Liu, H. Pan, M. Gao, Q. Wang, Advanced hydrogen storage alloys for Ni/MH rechargeable batteries, J. Mater. Chem. 21 (2011) 4743–4755. doi:10.1039/c0jm01921f.

[3] Y. Liu, Y. Cao, L. Huang, M. Gao, H. Pan, Rare earth-Mg-Ni-based hydrogen storage alloys as negative electrode materials for Ni/MH batteries, J. Alloys Compd. 509 (2011) 675–686. doi:10.1016/j.jallcom.2010.08.157.

[4] J. Liu, S. Han, Y. Li, L. Zhang, Y. Zhao, S. Yang, B. Liu, Phase structures and electrochemical properties of La–Mg–Ni-based hydrogen storage alloys with superlattice structure, Int. J. Hydrogen Energy. 41 (2016) 20261–20275. doi:10.1016/j.ijhydene.2016.08.149.

[5] T. Kohno, H. Yoshida, F. Kawashima, T. Inaba, I. Sakai, M. Yamamoto, M. Kanda, Hydrogen storage properties of new ternary system alloys: La_2MgNi_9, $La_5Mg_2Ni_{23}$, La_3MgNi_{14}, J. Alloys Compd. 311 (2000) 5–7. doi:10.1016/S0925-8388(00)01119-1.

[6] B. Liao, Y.Q. Lei, G.L. Lu, L.X. Chen, H.G. Pan, Q.D. Wang, The electrochemical properties of $La_xMg_{3-x}Ni_9$ (x = 1.0-2.0) hydrogen storage alloys, J. Alloys Compd. 356–357 (2003) 746–749. doi:10.1016/S0925-8388(03)00083-5.

[7] B. Liao, Y.Q. Lei, L.X. Chen, G.L. Lu, H.G. Pan, Q.D. Wang, Effect of the La/Mg ratio on the structure and electrochemical properties of $La_xMg_{3-x}Ni_9$ (x = 1.6 -2.2) hydrogen storage electrode alloys for nickel-metal hydride batteries, J. Power Sources. 129 (2004) 358–367. doi:10.1016/j.jpowsour.2003.11.044.

[8] V.V. Shtender, V.V. Pavlyuk, O.Y. Zelinska, W. Nitek, V. Paul-Boncour, G.S. Dmytriv, W. Łasocha, I.Y. Zavaliy, The Y–Mg–Co ternary system: alloys synthesis, phase diagram at 500 °C and crystal structure of the new compounds, J. Alloys Compd. 812 (2020). doi:10.1016/j.jallcom.2019.152072.

[9] V.V. Shtender, R.V. Denys, V. Paul-Boncour, I.Y. Zavaliy, Y.V. Verbovytskyy, D.D. Taylor, Crystal structure, hydrogen absorption-desorption behavior and magnetic properties of the $Nd_{3-x}Mg_xCo_9$ alloys, J. Alloys Compd. 695 (2017) 1426–1435. doi:10.1016/j.jallcom.2016.10.268.

[10] V.V. Shtender, R.V. Denys, I.Y. Zavaliy, O.Y. Zelinska, V. Paul-Boncour, V.V. Pavlyuk, Phase equilibria in the Tb-Mg-Co system at 500°C, crystal structure and hydrogenation properties of selected compounds, J. Solid State Chem. 232 (2015) 228–235. doi:10.1016/j.jssc.2015.09.031.

[11] T.N. Lamichhane, V. Taufour, A. Palasyuk, Q. Lin, S.L. Bud'Ko, P.C. Canfield, $Ce_{3-x}Mg_xCo_9$: Transformation of a Pauli Paramagnet into a Strong Permanent Magnet, Phys. Rev. Appl. 9 (2018) 24023. doi:10.1103/PhysRevApplied.9.024023.

[12] R. V. Denys, A.B. Riabov, R. Černý, I. V. Kovalchuk, I.Y. Zavaliy, New $CeMgCo_4$ and Ce_2MgCo_9 compounds: Hydrogenation properties and crystal structure of hydrides, J. Solid State Chem. 187 (2012) 1–6. doi:10.1016/j.jssc.2011.10.040.

[13] T.N. Lamichhane, V. Taufour, A. Palasyuk, S.L. Bud'ko, P.C. Canfield, Study of the ferromagnetic quantum phase transition in $Ce_{3-x}Mg_xCo_9$, Philos. Mag. 100 (2020) 1607–1619. doi:10.1080/14786435.2020.1727973.

[14] T. Pandey, D.S. Parker, Borderline Magnetism: How Adding Mg to Paramagnetic $CeCo_3$ Makes a 450-K Ferromagnet with Large Magnetic Anisotropy, Phys. Rev. Appl. 10 (2018) 034038. doi:10.1103/PhysRevApplied.10.034038.

[15] J. Rodriguez-Carvajal, Recent developments in the program FullProf, in commission on powder diffraction (IUCr), Newsletter. 26 (2001) 12–19.

[16] I. Bigun, M. Dzevenko, L. Havela, Y. Kalychak, *RE*Ni_9In_2 (*RE* = rare-earth metal): Crystal chemistry, hydrogen absorption, and magnetic properties, Eur. J. Inorg. Chem. 2014 (2015) 2631–2642. doi:10.1002/ejic.201400058.

[17] V.V. Shtender, V. Paul-Boncour, R.V. Denys, J.-C. Crivello, I.Y. Zavaliy, $TbMgNi_{4-x}Co_x$–$(H,D)_2$ System. I: Synthesis, Hydrogenation Properties, and Crystal and Electronic Structures, J. Phys. Chem. C. 124 (2020) 196–204. doi:10.1021/acs.jpcc.9b10252.

[18] M. Merches, W.E. Wallace, R.S. Craig, Magnetic and structural characteristics of some 2:17 rare earth-cobalt systems, J. Magn. Magn. Mater. 24 (1981) 97–105. doi:10.1016/0304-8853(81)90106-2.

[19] Z.G. Sun, H.W. Zhang, S.Y. Zhang, B.G. Shen, Structure and magnetic properties of $Nd_2(Co,Mn)_{17}$ compounds, Phys. B Condens. Matter. 305 (2001) 127–134. doi:10.1016/S0921-4526(01)00601-9.

[20] J.L. Girardet, A. Blaise, J. Chappert, J.J. Lawrence, J. Feron, J.C. Picoche, Magnetic and

crystallographic properties of ferritin, J. Appl. Phys. 41 (1970) 1002. doi:10.1063/1.1658785.
[21] T. Goto, H. Aruga Katori, T. Sakakibara, M. Yamaguchi, Successive phase transitions in ferromagnetic YCo_3, Phys. B. 177 (1992) 255–258. doi:10.1016/0921-4526(92)90107-4.
[22] X.Y. Cui, J. Liu, P.A. Georgiev, I. Morrison, D. Keith Ross, M.A. Roberts, K.A. Andersen, M. Telling, D. Fort, Effect of H on the crystalline and magnetic structures of the YCo_3–H(D) system. I. YCo_3 from neutron powder diffraction and first-principles calculations, Phys. Rev. B - Condens. Matter Mater. Phys. 76 (2007) 1–9. doi:10.1103/PhysRevB.76.184443.
[23] T. Goto, K. Fukamichi, T. Sakakibara, H. Komatsu, Itinerant electron metamagnetism in YCo_2, Solid State Commun. 72 (1989) 945–947. doi:10.1016/0038-1098(89)90433-X.
[24] G. Wiesinger, G. Hilscher, Magnetism of hydrides, in: K.H.J. Buschow (Ed.), Handb. Magn. Mater., Elsevier North-Holland, Amsterdam, 1991: p. 511.
[25] M.I. Bartashevich, K. Koui, T. Goto, M. Yamaguchi, I. Yamamoto, F. Sugaya, Magnetic properties of $NdCo_3$ and its γ-phase hydride $NdCo_3H_{4.1}$, J. Alloys Compd. 202 (1993) 7–12. doi:10.1016/0925-8388(93)90508-K.
[26] C. Kittel, Introduction To Solid State Physics, 8th ed., WILEY, 2005.
[27] Z. Budrikis, Magnetism: Doping rehabilitates failed materials, Nat. Rev. Mater. 3 (2018) 18018. doi:10.1038/natrevmats.2018.18.